

RESEARCH

Open Access



Analysis on LUT based digital predistortion using direct learning architecture for linearizing power amplifiers

Xiaowen Feng^{1,2}, Yide Wang^{1,3}, Bruno Feuvrie^{1,4}, Anne-Sophie Descamps^{1,4}, Yuehua Ding^{5,3*} and Zhiwen Yu^{3,6}

Abstract

In modern wireless communication system, power amplifier (PA) is an important component which is expected to be operated at the region of high power efficiency, but in this region, PA is inherently nonlinear. Thus, the linearization of high power efficient PA is necessary. In this paper, direct learning architecture (DLA) and indirect learning architecture (ILA) are firstly compared. It shows that DLA is more robust than ILA. Then a baseband digital predistortion (DPD) method with DLA is proposed for power amplifier linearization based on combined look-up tables (LUT) and memory polynomial (MP) model. The main innovation is that a LUT-based approach is proposed to calculate directly the complex-valued predistorted signal. Moreover, some interpolation techniques are introduced to reduce the LUT size. The proposed DPDs are validated experimentally. Additionally, the influences of some important parameters in experimental setup, such as the number of bits of analog-to-digital converter (ADC) and the instrument bandwidth, are analyzed.

Keywords: Baseband digital predistortion, Power amplifiers, Memory polynomial, Look-up table

1 Introduction

In modern wireless communication system, the energy consumption is an extremely important issue, especially for the transmitter. Power amplifier (PA) is a crucial component in the transmitter. Generally, for achieving a good power efficiency, PA must operate close to its compression region. Unfortunately, the high spectral efficiency signals used by today's wireless communication systems are characterized by their non-constant envelopes and high peak-to-average power ratio (PAPR). Their amplitudes may overtop the compression region of the PA. The resulting nonlinear distortions, such as the spectral regrowth and degradation of error vector magnitude (EVM), disturb the transmission. Moreover, to support

more users and provide higher data rates, the bandwidth of signal continues to increase. PA exhibits stronger memory effects with the increasing of the bandwidth of signal [1]. The research on high power efficient PA driven by a wide bandwidth signal is of great practical significance [2, 3]. To compensate PA nonlinearities, several linearization techniques are developed, such as feed-forward, feedback, linear amplification with nonlinear components (LINC) and predistortion techniques. Among these techniques, predistortion technique, particularly baseband digital predistortion (DPD), has been widely studied thanks to its ability of reconfiguration and simplicity of implementation.

DPD is one of the most effective linearization techniques. Its principle is to insert a digital predistorter (PD) in front of PA, which has the inverse nonlinear characteristics of that of the PA, so that the cascaded PD-PA system has a linear behavior. DPD can be realized using two architectures [4–6]: indirect learning architecture (ILA) and direct learning architecture (DLA). In ILA approach [7], a postdistorter model is first assumed, the measured output of PA is taken as the input of the

*Correspondence: eeyhdng@scut.edu.cn

⁵ School of Electronic and Information Engineering, South China University of Technology, Wushan Road, Tianhe District, Guangzhou, Peoples Republic of China

³ Sino-French Research Center in Information and Communication (SFC/RIC), Rue Christian Pauc, Nantes, France

Full list of author information is available at the end of the article

postdistorter, and the measured input of PA is taken as the output of the postdistorter. Then, the postdistorter is estimated by an identification algorithm such as least squares (LS) method. Finally, the identified postdistorter is placed directly in front of PA as the predistorter. In DLA approach [8–10], a model of PA's behavior is first defined, then its coefficients are identified, and finally the predistorter is found by reversing the identified PA model.

Among various DPD techniques, three solutions are popularly used. They are look-up table (LUT), polynomial model and neural network based DPDs. In [11, 12], several neural network-based DPDs have been proposed. The neural network has an excellent capability to accurately approximate nonlinear functions. Hence, it can be used to linearize the PA. But the training process of neural network is complex and time-consuming. Its hardware implementation is difficult in practical applications. LUT [13–16] based DPD has the advantage of simplicity, but its linearization performance depends on the LUT size. In order to improve the linearization performance with limited LUT dimension, some interpolated techniques are introduced in LUT-based DPDs. Polynomial [7, 8, 17] model-based DPD is also widely studied in the literature. They include the well-known Volterra series (VS) [18], memory polynomial (MP) [7, 8, 13], generalized memory polynomial (GMP) [19], other simplified VS variants [20] and so on. VS and GMP models are more accurate but also more complex. MP model has lower complexity and can closely mimic the nonlinear behavior of the PA with memory effects. It offers a good tradeoff between computational complexity and modeling accuracy.

In [7], a MP based DPD with indirect learning architecture is presented, where the MP model performs robustly and the model's parameters are easy to extract. But compared with the DPD with direct learning architecture, the DPD with indirect learning architecture is less robust in the presence of noise [4]. In [10], a MP-based DPD with direct learning architecture is proposed, where it uses a root-finding method to calculate the predistorted signal. This DPD can achieve excellent linearization performance but the root-finding procedure is time-consuming. In [13], a MP/LUT DPD is proposed, where a conventional LUT is used instead of the root-finding procedure. The calculating time of DPD process decreases greatly but it requires a sufficiently large size of LUT.

In our previous work [21, 22], some interpolated LUTs are introduced based on MP/LUT DPD. Thanks to the interpolation techniques, the improved DPDs achieve good performance in terms of computational efficiency and LUT size. In [21], the linear interpolation is introduced based on MP/LUT DPD. In [22], the

quadratic-interpolated LUT is combined with the non-uniform MP model. It is worth noting that, in [21, 22], LUTs are only used to determine the amplitude of the predistorted signal. While the predistorted signal's phase must be calculated by another separated time-consuming process. In [23], the two interpolated LUTs are used based on non-uniform MP model. The linear-interpolated LUT is used to determine the amplitude of the predistorted signal. And, the quadratic-interpolated LUT is used to determine the phase of the predistorted signal. In this paper, we propose three LUT-based methods: LUT-based, LILUT-based, and QILUT-based methods. In the LUT-based method, the amplitude and phase of the predistorted signal both are calculated by a single classical LUT. In the LILUT-based method, the amplitude and phase of the predistorted signal both are calculated by a single linear-interpolated LUT. In the QILUT-based method, the amplitude and phase of the predistorted signal both are calculated by a single quadratic-interpolated LUT.

Additionally, in practical implementation, the linearization performance of DPDs is directly related to the number of bits of ADC (analog-to-digital converter) and the bandwidth of instruments [24]. This important issue is also studied in this paper.

The remainder of this paper is organized as follows. Section 2 presents the principles of ILA and DLA, and makes a comparison between them. The proposed DPD solution is presented in Section 3. Section 4 discusses some practical problems in the measurements, especially the influence of signal bandwidth. The experimental setup and results are presented in Section 5. Finally, Section 6 concludes the paper.

2 Predistortion architectures

In this section, the details of ILA and DLA are presented. And, the two architectures are compared by some simulations.

2.1 Indirect learning architecture

Figure 1 shows the block diagram of ILA. Firstly, the postdistorter is identified. Usually, the postdistorter is modeled as a MP [4]. The output of the postdistorter can be expressed as

$$z_p(n) = \sum_{k=0}^K \sum_{l=0}^L a_{kl} \Phi_{kl}[z(n)] \quad (1)$$

where $z(n) = \frac{y(n)}{G_0}$, $\Phi_{kl}[z(n)] = z(n-k)|z(n-k)|^{2l}$, G_0 is the desired gain, a_{kl} ($k = 0, \dots, K$ and $l = 0, \dots, L$) are the complex-valued coefficients, K refers to the memory depth and $2L + 1$ the highest nonlinearity order. Theoretically, it requires $z_p(n) = x(n)$ in a perfect system. The

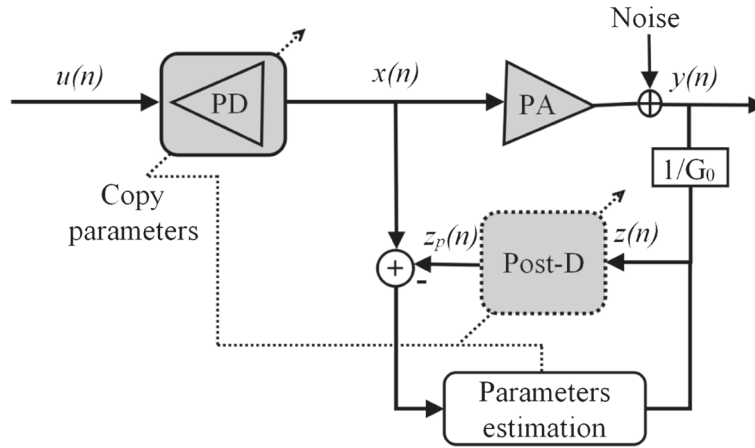


Fig. 1 Indirect learning architecture

signals $x(n)$ and $y(n)$ are the measured input and output of PA, respectively. Assume that the total number of samples is N , we get

$$\mathbf{z}_p = \mathbf{Z}\mathbf{a} \quad (2)$$

where $\mathbf{z}_p = [z_p(1), \dots, z_p(N)]^T$, $\mathbf{Z} = [\mathbf{u}_{00}, \dots, \mathbf{u}_{0L}, \dots, \mathbf{u}_{KL}, \dots, \mathbf{u}_{K0}, \dots, \mathbf{u}_{KL}]_{N \times (K+1)(L+1)}$, $\mathbf{u}_{kl} = [\Phi_{kl}[z(1)], \dots, \Phi_{kl}[z(N)]]^T$, and $\mathbf{a} = [a_{00}, \dots, a_{0L}, \dots, a_{KL}, \dots, a_{K0}, \dots, a_{KL}]^T$. Classical LS method can be used to extract the coefficients

$$\hat{\mathbf{a}} = (\mathbf{Z}^H \mathbf{Z})^{-1} \mathbf{Z}^H \mathbf{z}_p \quad (3)$$

where $(\cdot)^H$ denotes the complex conjugate transpose operation. After the identification of the postdistorter, the copy of the postdistorter is placed directly in front of PA as the predistorter.

2.2 Direct learning architecture

The block diagram of DLA is illustrated in Fig. 2. As mentioned before, the determination of PD needs two steps in

DLA. Firstly, the model of PA's behavior needs to be pre-defined. Here, MP is adopted as the PA model. The PA model is defined as

$$y(n) = \sum_{p=0}^P \sum_{q=0}^Q c_{pq} \Phi_{pq}[x(n)] \quad (4)$$

where $\Phi_{pq}[x(n)] = x(n-p) |x(n-p)|^{2q}$, P and $2Q+1$ are the memory depth and highest nonlinearity order, respectively, and c_{pq} are the model's coefficients. The signals $x(n)$ and $y(n)$ are the input and output of PA, respectively. The coefficients c_{pq} are extracted by LS method as mentioned before. Secondly, the identified model of PA is reversed for the determination of PD. In the following, the method in [10] to determine the PD with DLA is described.

The ideal cascaded PD-PA system can be expressed as

$$y(n) = \sum_{p=0}^P \sum_{q=0}^Q c_{pq} \Phi_{pq}[x(n)] = G_0 u(n) \quad (5)$$

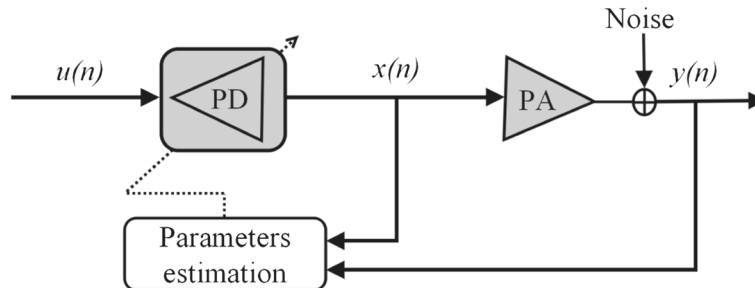


Fig. 2 Direct learning architecture

where $u(n)$ denotes the input of the PD-PA system and $x(n)$ the predistorted signal (also the input of PA). According to the memory behavior of PA, the output $y(n)$ of PA can be represented as the sum of two parts: the static part $s(n)$ depending only on the current input sample ($p = 0$), and the dynamic part $d(n)$ which depends on the previous input samples (p from 1 to P).

$$\begin{cases} y(n) = s(n) + d(n) \\ s(n) = \sum_{q=0}^Q c_{0q} \Phi_{0q}[x(n)] \\ d(n) = \sum_{p=1}^P \sum_{q=0}^Q c_{pq} \Phi_{pq}[x(n)] \end{cases} \quad (6)$$

From (5) and (6), $s(n)$ can be rewritten as

$$s(n) = e^{j\angle x(n)} \sum_{q=0}^Q c_{0q} |x(n)|^{2q+1} = G_0 u(n) - d(n) \quad (7)$$

where $\angle x(n)$ and $|x(n)|$ are the phase and amplitude of the predistorted signal $x(n)$, respectively. By definition, $d(n)$ depends only on the previous samples, the right-hand side of (7) and coefficients c_{0q} are known at instant n . The amplitude $|x(n)|$ of the predistorted signal can be calculated by taking the absolute value.

$$\left| \sum_{q=0}^Q c_{0q} |x(n)|^{2q+1} \right| = |G_0 u(n) - d(n)| \quad (8)$$

Equation (8) is a high-order nonlinear equation, the amplitude $|x(n)|$ of the predistorted signal can be found by a root-finding procedure [10]. The corresponding phase $\angle x(n)$ is then calculated by

$$\angle x(n) = \arg \left\{ \frac{G_0 u(n) - d(n)}{\sum_{q=0}^Q c_{0q} |x(n)|^{2q+1}} \right\}. \quad (9)$$

Finally, the predistorted signal $x(n)$ is given by

$$x(n) = |x(n)| e^{j\angle x(n)}. \quad (10)$$

2.3 Comparison of ILA and DLA

Two different DPD architectures (ILA and DLA) are presented in the above subsection. They both need to identify a pre-assumed model (MP model) with the measured input and output of PA. LS method is used in the model identification. From (3), it can be seen that the inverse of $\mathbf{Z}^H \mathbf{Z}$ is required in LS algorithm. When solving the inverse problem, the condition number is usually used to measure how sensitive the solution is to changes or errors in the input. A problem with a low condition number is said to be well-conditioned, while a problem with a high condition number is said to be ill-conditioned.

In this subsection, the condition number of $\mathbf{Z}^H \mathbf{Z}$ is considered to measure the stability of the two DPD architectures. In ILA, \mathbf{Z} is related to the output signal of PA. While in DLA, it is related to the input signal of PA. A simulation is realized to compare these

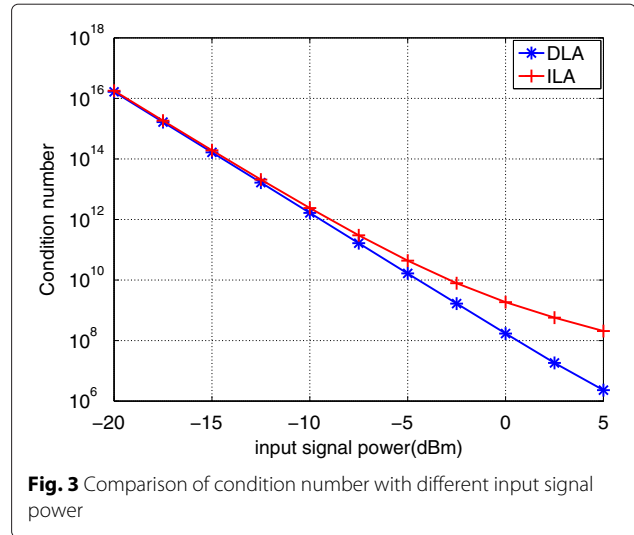


Fig. 3 Comparison of condition number with different input signal power

two DPD architectures. In this simulation, a Wiener model is used as PA model. It is implemented as a three-tap FIR filter with coefficients [0.7692, 0.1538, 0.0769] [25], followed by a Saleh model. Saleh model is described as

$$y(n) = \frac{\alpha_a |v(n)|}{1 + \beta_a |v(n)|^2} e^{j\angle[v(n) + \frac{\alpha_p |v(n)|^2}{1 + \beta_p |v(n)|^2}]} \quad (11)$$

where $y(n)$ and $v(n)$ are the output and input of Saleh model, respectively, and $\alpha_a = 20$, $\beta_a = 2.2$, $\alpha_p = 2$, $\beta_p = 1$ [26]. The input signal of PA is a WCDMA signal with 3.84 MHz bandwidth. The measured sequence has 1000 symbols (8000 samples). The ideal gain of this PA model is about 26 dB. The input power at 1 dB compression point is about -1 dBm.

The condition number of $\mathbf{Z}^H \mathbf{Z}$ is affected by \mathbf{Z} which depends on the memory depth, nonlinearity order and value of each element (varies with the input signal power). In the first simulation, we assume that the memory depth is 3 ($K = P = 3$) and the nonlinearity order is 5 ($L = Q = 2$). The signal input power varies from -20 to 5 dBm. The condition numbers of $\mathbf{Z}^H \mathbf{Z}$ of two DPD architectures are compared. The results are shown in Fig. 3.

In the second simulation, we assume that the input signal power is 0 dBm. The nonlinearity order varies from 3 to 15. The memory depth varies from 0 to 3. The comparison of two DPD architectures is shown in Fig. 4.

From Figs. 3 and 4, it can be seen that the condition number of $\mathbf{Z}^H \mathbf{Z}$ in DLA is always lower than that in ILA. It indicates that DLA is more robust than ILA with respect to perturbations. To further validate this result, the influences of the noise and quantization error of ADC on the modeling performance are analyzed.

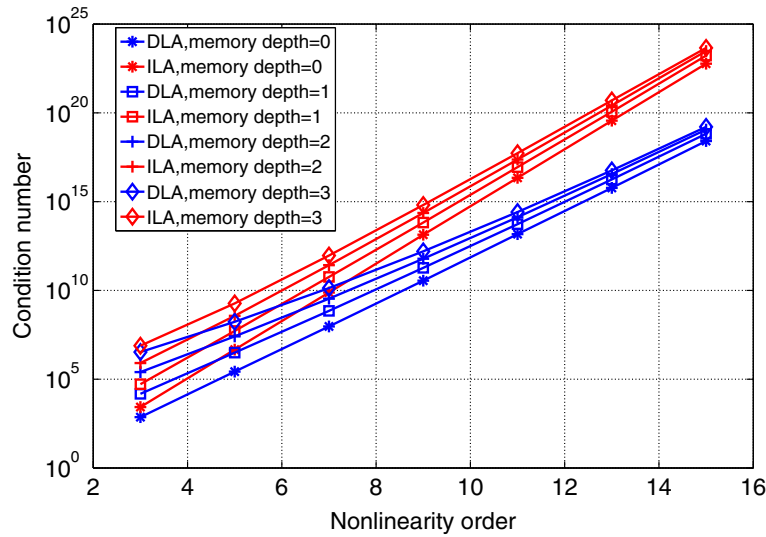


Fig. 4 Comparison of condition number with different nonlinearity orders and memory depths

In practical measurement, an ADC is required to realize the signal acquisition. The number of bits of ADC will affect the accuracy of the signal acquisition and then affect the performance of the model's identification. Additionally, the measurement at the output of PA is noisy in practical application. The noise also affects the performance of the model's identification. In the third simulation, these two DPD architectures are compared in terms of the number of bits of ADC in signal acquisition and the noise power at the output of PA.

For analyzing the influence of the noise at the output of PA, it assumes that complex white Gaussian noise is

present at the output of PA as shown in Figs. 1 and 2. An original WCDMA signal $x'(n)$ (bandwidth 3.84 MHz, power 0 dBm, sequence length 8000 samples) is given as the PA input. And the output $y'(n)$ of PA is obtained by the Wiener model. The white Gaussian noise is added in the output signal $y'(n)$ to get the noisy output $y'_{noise}(n)$. The input $x'(n)$ and output $y'_{noise}(n)$ of PA are used for the model identification of (1) and (4). In this process, we take $K = P = 3$ (memory depth = 3) and $L = Q = 2$ (nonlinearity order = 5), respectively.

After the model identification, another WCDMA signal $x''(n)$ is used to test the identified model. For the input $x''(n)$, the corresponding output $y''(n)$ is obtained.

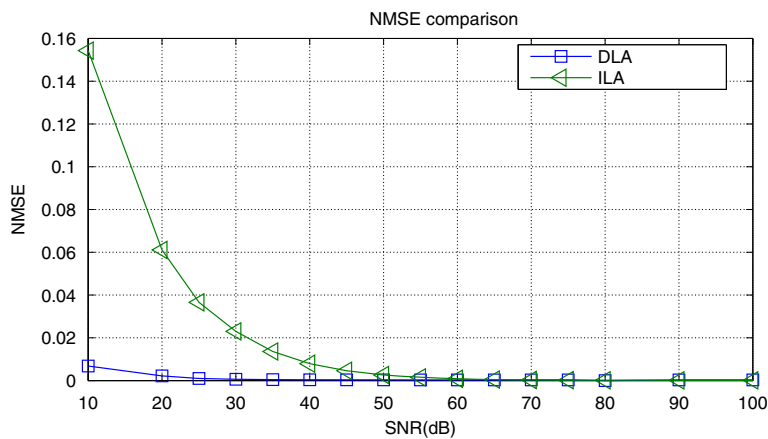


Fig. 5 Comparison of ILA and DLA when considering the noise

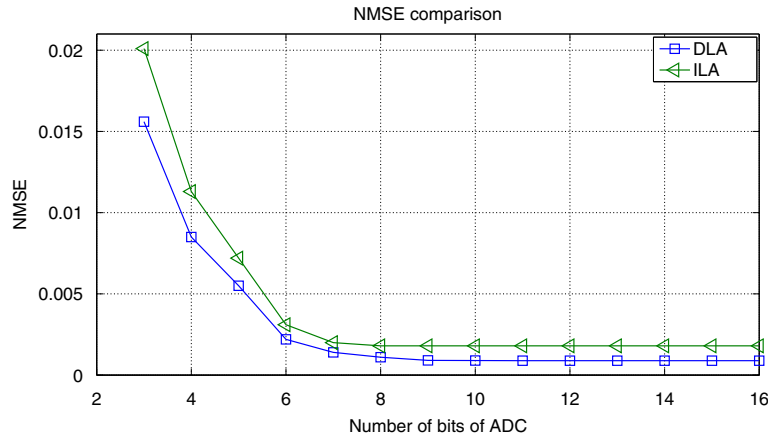


Fig. 6 Comparison of ILA and DLA when considering the number of bits of ADC

For ILA, the signal $y''(n)$ is the input of the postdistorter, its output $z_p''(n)$ is obtained by the identified model (1). The normalized mean squared error (NMSE) between $z_p''(n)$ and $x''(n)$ is treated as the criterion of ILA modeling accuracy. For DLA, the signal $x''(n)$ is the input of the identified model (4), the corresponding output $y_{DLA}''(n)$ is obtained. The normalized mean squared error (NMSE) between $y_{DLA}''(n)$ and $y''(n)$ is treated as the criterion of DLA modeling accuracy. Figure 5 shows the performance of ILA and DLA in terms of NMSE when the noise is present. It can be seen that the modeling accuracy of ILA and DLA both improves as the noise power decreases. When the noise is high, the performance of DLA is better than that of ILA. When the power of noise is low (nearly ideal case), the performance of DLA and ILA is similar. In practical applications, the noise can not be ignored. DLA is more robust than ILA when the noise is present.

For the influence of the number of bits of ADC, an ADC is assumed for the signal acquisition. The signals $x'(n)$

and $y'(n)$ pass the ADC and are denoted by $x'_{ADC}(n)$ and $y'_{ADC}(n)$, respectively. The signals $x'_{ADC}(n)$ and $y'_{ADC}(n)$ are used for the model identification of (1) and (4). The same signal $x''(n)$ is used to test the identified model. The comparison principle considering the number of bits of ADC is the same as that considering the noise. Figure 6 shows the performance of ILA and DLA in terms of NMSE with varying number of bits of ADC. It can be seen that the modeling accuracy of ILA and DLA both improves as the number of bits of ADC increases. The modeling accuracy of DLA is always better than that of ILA.

According to the above analysis, it further verifies that DLA is more robust than ILA with respect to perturbations. Finally, the two DPDs based on different learning architectures are compared for the validation. The DPD proposed in [7] is taken as the example of ILA. And, the DPD proposed in [10] is taken as the example of DLA. In this simulation, the number of bits of ADC and the noise

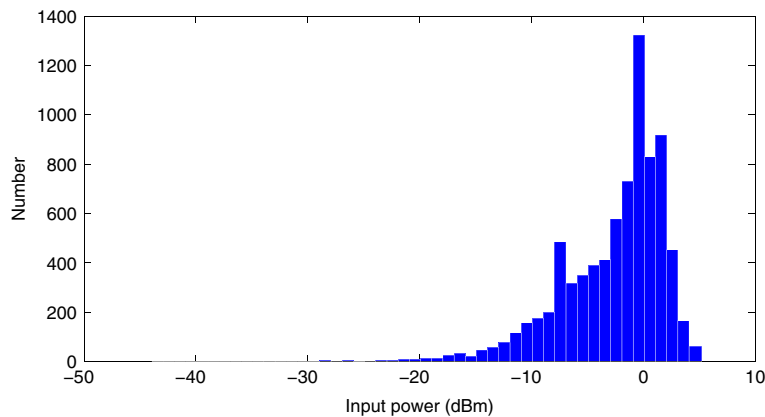


Fig. 7 Histogram distribution of the input signal when the average power is -3 dBm

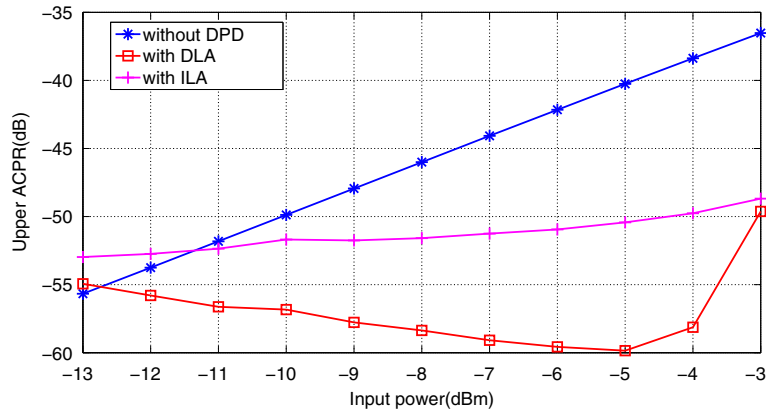


Fig. 8 ACPR comparison of DPDs based different learning architectures

both are taken into account in the process of identification. We assume that the number of bits of ADC is 8, the SNR at the output of PA is 35 dB. The average power of the input signal varies from -13 to -3 dBm. The input signal, which has an average power of -3 dBm, includes many samples entering the nonlinear region of PA model. Figure 7 illustrates the distribution of samples of the input signal when its average power is -3 dBm. It shows that the power of about 40 % of the input samples is higher than the input power (-1 dBm) at 1 dB compression point of the PA model.

The original input $x'(n)$ and output $y'(n)$ of PA pass firstly the ADC, then the noise is added on the output signal of PA. The processed input and output signals are used for the model identification of (1) and (4). For ILA, the identified postdistorter model is directly placed in front of PA as the predistorter [7]. For DLA, the predistorter is determined by inverting the identified PA model [10].

The linearized outputs of the two different learning architectures are obtained by the DPD solutions stated above. The adjacent channel power ratio (ACPR) and EVM of linearized outputs of two architectures are calculated, respectively. Figure 8 shows the evolution of ACPR of linearized outputs with varying input power. And, Fig. 9 shows the evolution of EVM of linearized outputs with varying input power. It can be seen that the linearization performance of DLA is much better than that of ILA when considering the number of bits of ADC and the noise at the output of PA. Consequently, in this paper, DPD based on DLA is adopted.

3 Proposed LUT-based digital predistortion

In this section, the details of the proposed DPD are presented. In Section 2.2, a MP-based DPD with DLA is described. The calculation of the predistorted signal includes two parts: the amplitude and phase. The amplitude and phase of the predistorted signal are calculated by

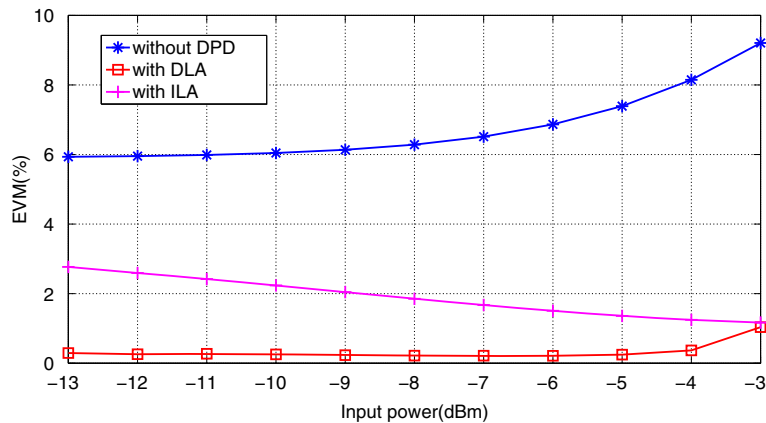


Fig. 9 EVM comparison of DPDs based different learning architectures

Table 1 Values of LUT

LUT input	LUT output
$E(0)$	$R(0)e^{j\theta(0)}$
...	...
$E(m)$	$R(m)e^{j\theta(m)}$
...	...
$E(M)$	$R(M)e^{j\theta(M)}$

(8) and (9), respectively. In [13, 21, 22], only the amplitude calculation in (8) is considered. The approaches based on LUT are used instead of the root-finding process. Actually, the process of calculating the phase in (9) is also time-consuming. In this paper, an approach based on LUT is proposed to calculate the amplitude and also the phase of the predistorted signal. The proposed approach is presented as follows. (9) can be rewritten as

$$\angle x(n) = \arg \{G_0 u(n) - d(n)\} - \arg \left\{ \sum_{q=0}^Q c_{0q} |x(n)|^{2q+1} \right\}. \quad (12)$$

Before performing the predistortion, a LUT including the information of the amplitude and phase of the predistorted signal should be constructed. Firstly, the dynamic range of the amplitude $|x(n)|$ of the predistorted signal is estimated according to the maximum amplitude of the original input signal $u(n)$ and the saturation input amplitude of PA. Then the maximum range of $|x(n)|$ is decomposed into $M + 1$ intervals with equal length (the length of each interval is equal to Δx), denoted by $R(m)$. The LUT is shown in Table 1. In this table,

$$R(m) = m\Delta x \quad (13)$$

$$E(m) = \left| \sum_{q=0}^Q c_{0q} R(m)^{2q+1} \right| \quad (14)$$

$$\theta(m) = \arg \left\{ \sum_{q=0}^Q c_{0q} R(m)^{2q+1} \right\} \quad (15)$$

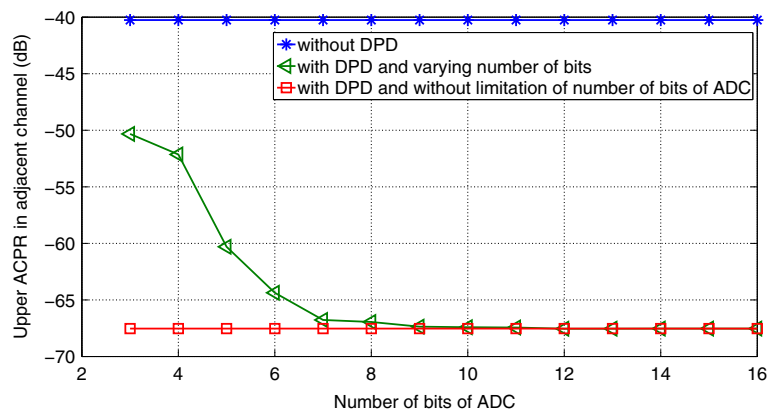
where $E(m)$ is the LUT input and $\theta(m)$ the phase of the term $\sum_{q=0}^Q c_{0q} R(m)^{2q+1}$.

After the LUT is constructed, the predistortion algorithm is described in Algorithm 1.

Algorithm 1 Proposed DPD based on simple LUT

1. Initialize $n = 0$, $d(0) = 0$.
Begin loop
{
 2. Calculate the value of $G_0 u(n) - d(n)$, denoted by $s(n)$.
 3. Find a value $E(m)$ from Table 1, which is the closest to $|s(n)|$.
 4. Find the corresponding value of $x(n)$ by $x(n) = LUT\{E(m)\} = R(m)e^{j[\arg\{s(n)\} - \theta(m)]}$
 5. Calculate $n = n + 1$.
 6. Calculate $d(n) = \sum_{p=1}^P \sum_{q=0}^Q c_{pq} x(n-p) |x(n-p)|^{2q}$.
} Goto loop
-

The proposed approach based on a simple LUT can significantly improve the time efficiency of DPD process than the corresponding root-finding approach, but its linearization performance is proportional to the table size. To obtain good linearization performance, the table size must be sufficiently large. Therefore, some interpolation techniques should be introduced in the simple LUT. The linear interpolation and the quadratic interpolation

**Fig. 10** Evolution of adjacent channel ACPR versus number of bits of ADC

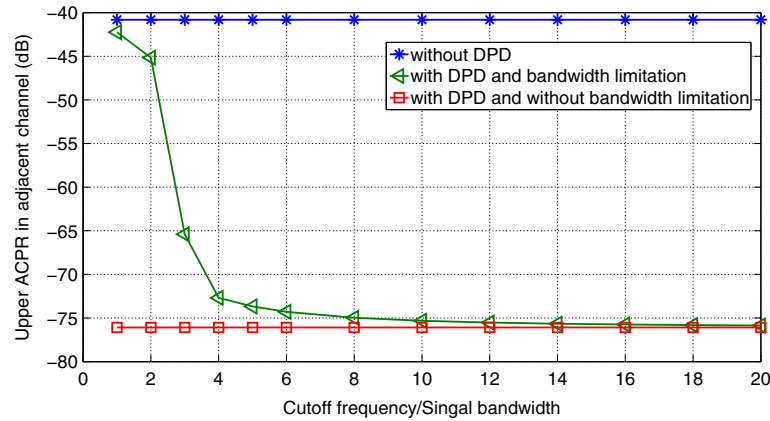


Fig. 11 Evolution of adjacent channel ACPR versus cutoff frequency

are adopted in LUT, respectively. The linear-interpolated LUT and quadratic-interpolated LUT will be denoted in the rest of the paper as LILUT and QILUT, respectively. The algorithm of proposed DPD based on LILUT is different from that based on simple LUT at the step 4). For the algorithm of proposed DPD based on LILUT, the step 4) is as follows

$$x(n) = LILUT\{E(m)\} = R(m)e^{j\{\arg\{s(n)\} - \theta(m)\}} \quad (16)$$

where *LILUT* is the linear-interpolated LUT [21]. Similarly, for the algorithm of proposed DPD based on QILUT,

the step 4) is as follows

$$x(n) = QILUT\{E(m)\} = R(m)e^{j\{\arg\{s(n)\} - \theta(m)\}} \quad (17)$$

where *QILUT* is the quadratic-interpolated LUT [22].

In this section, three DPD approaches are described. For convenience, the proposed DPDs based on simple LUT, LILUT and QILUT are called as LUT-based, LILUT-based, and QILUT-based, respectively. Among these three approaches, it is difficult to judge which one is the best, since they provide different degrees of trade-off between the linearization performance, table size and time efficiency.

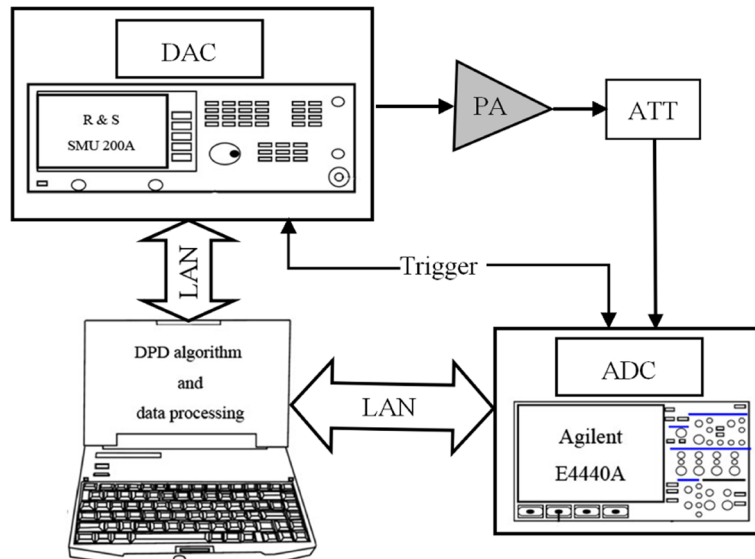


Fig. 12 Block diagram of experimental setup

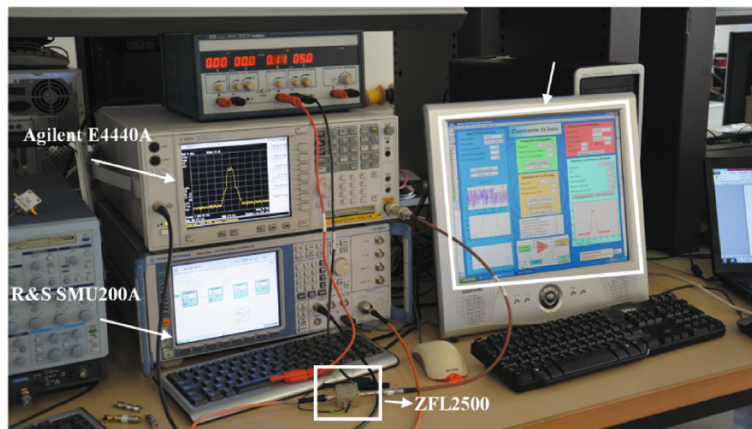


Fig. 13 Photograph of experimental setup

4 Discussions

In order to validate the proposed DPDs, experimental measurements are necessary. Before the measurements, some problems are discussed. In practical measurements, hardware conditions can not be ignored, such as the number of bits of ADC and instrument bandwidth. In the following, these parameters are analyzed by some simulations. In the simulations, the original input signal is a WCDMA signal with 3.84 MHz bandwidth. The input sequence is 1000 symbols. The input power is -5 dBm. The PA model is the Wiener PA model mentioned in Section 2.3. The DPD method used is the root-finding-based DPD [10].

For the problem of number of bits of ADC, as mentioned before, an ADC is assumed before the data

acquisition. The number of bits of ADC varies from 3 to 16. And the sampling frequency of the input signal is eight samples/symbol. The ACPR is used to quantify the linearization performance. Figure 10 presents the evolution of ACPR versus the number of bits of ADC. It can be seen that the linearization performance improves as the number of bits of ADC increases. It indicates that if the number of bits of ADC is not big enough in the data acquisition, the quantization error is too large and degrades the linearization performance. Additionally, the number of bits of ADC should not be too high. In this paper, the acquisition of signals by Agilent E4440A is realized with ADC of 14 bits in the experimental setup. The experimental setup will be presented in the next section.

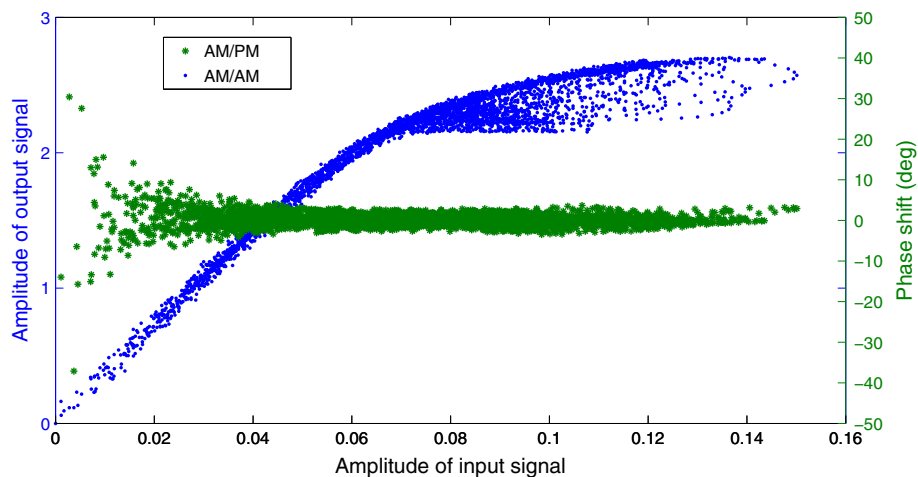


Fig. 14 AM/AM and AM/PM characteristics of PA ZFL2500

Another problem is the bandwidth of instrument. In simulations, the signal bandwidth is only limited by the sampling frequency. In the measurement, except for the influence of the sampling frequency, the signal bandwidth is also affected by the bandwidth of instrument. When the bandwidth of instrument is narrower than that of the signal, the signal passing the instrument will be distorted. Especially, the signal bandwidth will increase after the predistortion. The bandwidth of the predistorted signal is wider than that of the original input signal. Thus, if the bandwidth of instrument is not sufficiently wide, the desired predistortion will be not achieved.

In order to evaluate the required bandwidth, the following simulation is made. It assumes that the sampling frequency of input signal is 50 samples/symbol. To simulate the instrument limitation, a lowpass linear-phase filter, with order 200 and a varying cutoff frequency, is used to limit the bandwidth of the predistorted signal. The limited bandwidth signal is finally applied to the Wiener PA model.

Figure 11 presents the evolution of ACPR versus the cutoff frequency, where this cutoff frequency represents the bandwidth of instrument. It indicates that only the bandwidth of instrument is wide enough (at least 5 times), the linearization performance will be perfect.

5 Experimental results

In order to validate the proposed DPDs, an experimental testbed is built. Figures 12 and 13 show the used experimental testbed. It consists of a PA (ZFL 2500), a PC providing the baseband signal and realizing DPD algorithms, a vector signal generator (Rohde & Schwarz SMU 200 A) to generate the RF signal and a spectrum analyzer (Agilent E4440A, 3 Hz – 26.5 GHz) to analyze the input and output signals of PA. For PA ZFL2500, it has 500–2500 MHz bandwidth and about 31 dB gain. The average output power at 1 dB compression point is around 17 dBm at frequency of 1.8 GHz. Figure 14 shows AM/AM and AM/PM characteristics of PA ZFL2500.

The proposed approach, LUT-based, LILUT-based, and QILUT-based DPDs, all are tested on this experimental testbed. The root-finding-based DPD in [10] is compared with the proposed three DPD approaches. The performance is evaluated in terms of the linearization capability, time efficiency and table size. The linearization capability is measured by two parameters. One is the NMSE between the predistorted signals by the three LUT based DPDs and the predistorted signal by root-finding-based DPD. The other is the measured ACPR at the output of linearized PA. The time efficiency refers to the consumed time of DPD process

Table 2 NMSE of predistorted signals and time comparisons using different DPD methods

DPDs	NMSE (dB)	Time (us)
Root-finding-based DPD	$-\infty$	103.75
LUT-based DPD (size 30)	-34.18	9.63
LUT-based DPD (size 1000)	-65.39	11.38
LILUT-based DPD (size 10)	-61.20	20.75
LILUT-based DPD (size 30)	-81.59	21.38
QILUT-based DPD (size 10)	-75.93	71.25
QILUT-based DPD (size 20)	-94.89	72.88

for obtaining one predistorted sample $x(n)$ as shown in Algorithm 1. The table size refers to the chosen size of LUT.

For these measurements, PA ZFL2500 is driven by a WCDMA signal with 3.8 MHz bandwidth. The sampling frequency is 20 samples/symbol. The signal sequence has 200 symbols (4000 samples). The considered MP model has a memory depth and nonlinearity order of 3 and 5, respectively. The NMSE between the predistorted signal by the proposed LUT-based DPD and the predistorted signal by root-finding-based DPD and consumed time of the proposed LUT-based DPD are summarized in Table 2. The power of original signal is -14 dBm (the corresponding output power is 17 dBm at the output of PA). It can be seen that the NMSE between the root-finding-based DPD and QILUT-based DPD achieves -94.89 dB with table size of only 20. But, the consumed time of QILUT-based DPD is 72.88 us. It is higher than that of LILUT-based DPD (size 30) and that of LUT-based DPD (size 1000). The NMSE between the root-finding-based DPD and LILUT-based DPD achieves -81.59 dB when the table size is 30. The NMSE between the root-finding-based DPD and LUT-based DPD only achieves -65.39 dB even if the table size is up to 1000. But it takes only 11.38

Table 3 ACPR comparison using different DPD methods

Output power point	ACPR (dB)			
	17 dBm	16 dBm	15 dBm	14 dBm
Without DPD	-37.86	-40.23	-42.94	-45.08
Root-finding-based DPD	-43.45	-47.41	-50.79	-53.47
LUT-based DPD (size 30)	-39.53	-44.47	-45.70	-45.90
LUT-based DPD (size 1000)	-41.76	-47.58	-51.06	-53.59
LILUT-based DPD (size 10)	-39.33	-45.72	-50.91	-53.60
LILUT-based DPD (size 30)	-43.33	-45.75	-51.12	-53.53
QILUT-based DPD (size 10)	-41.59	-46.08	-50.84	-53.19
QILUT-based DPD (size 20)	-43.34	-47.52	-50.69	-53.86

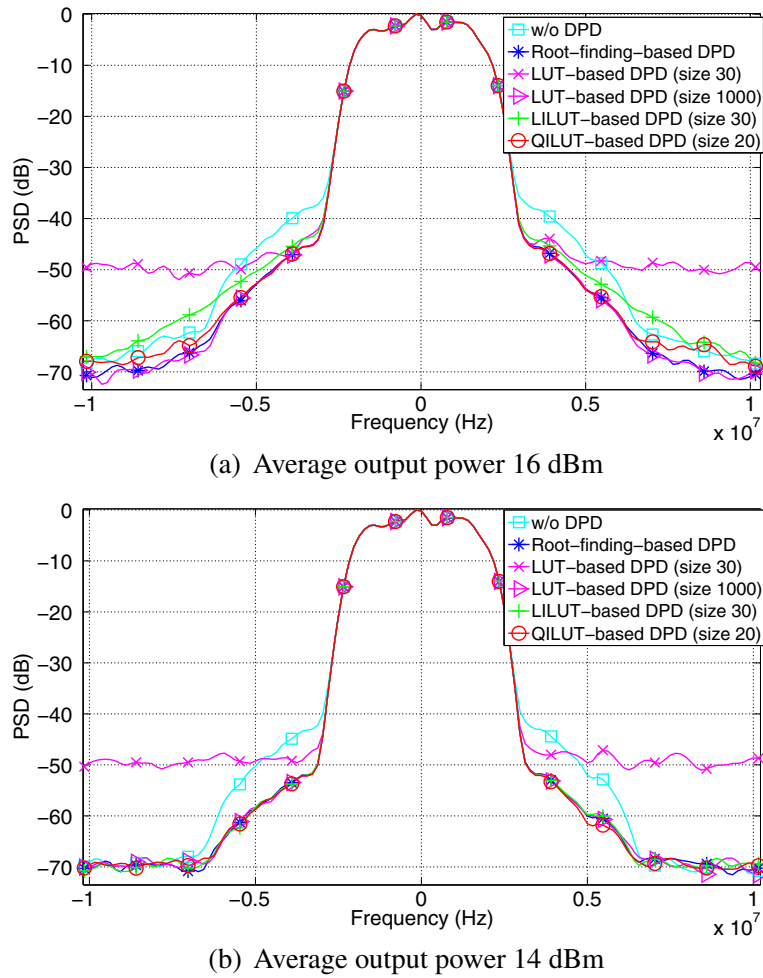


Fig. 15 Comparison of several DPDs

us. The advantage of LUT-based DPD is its high time efficiency.

To compare ACPR values at the output of linearized PA, four average output power points are chosen: 17, 16, 15 and 14 dBm. The upper ACPR values of the output signals of different DPDs are measured and summarized in Table 3 (the offset of adjacent channel is set to be 5 MHz). Figure 15 shows the spectrums of output signals using different DPDs at the output power point 16 and 14 dBm. The ACPR values and spectrums further validate the results of Table 2. For LUT-based DPD, the linearization performance is very low when the table size is small. It achieves a similar linearization performance as the root-finding-based DPD with table size at least 1000. While LILUT-based DPD and QILUT-based DPD achieve the same performance as the root-finding-based DPD, with table size of only 30 and 20, respectively. In order to compare LILUT-based DPD and QILUT-based DPD clearly,

Fig. 16 shows their spectrums with the same table size 10 at the output power point 16 and 14 dBm. At the output power 16 dBm, the linearization performance of QILUT-based DPD is better than that of LILUT-based DPD. It is worth noting that, the linearization performance of QILUT-based DPD is a little worse than that of LILUT-based DPD at the output power 14 dBm. It is because the characteristic at the output power 14 dBm is more linear than that at the output power 16 dBm. LILUT-based DPD is better for the case where the probability density of small signal is high (low nonlinearity). When the probability density of large signal is high, the nonlinearity increases, QILUT-based DPD can be selected.

6 Conclusions

Two classical DPD architectures (DLA and ILA) are compared in this paper. According to the comparison in terms

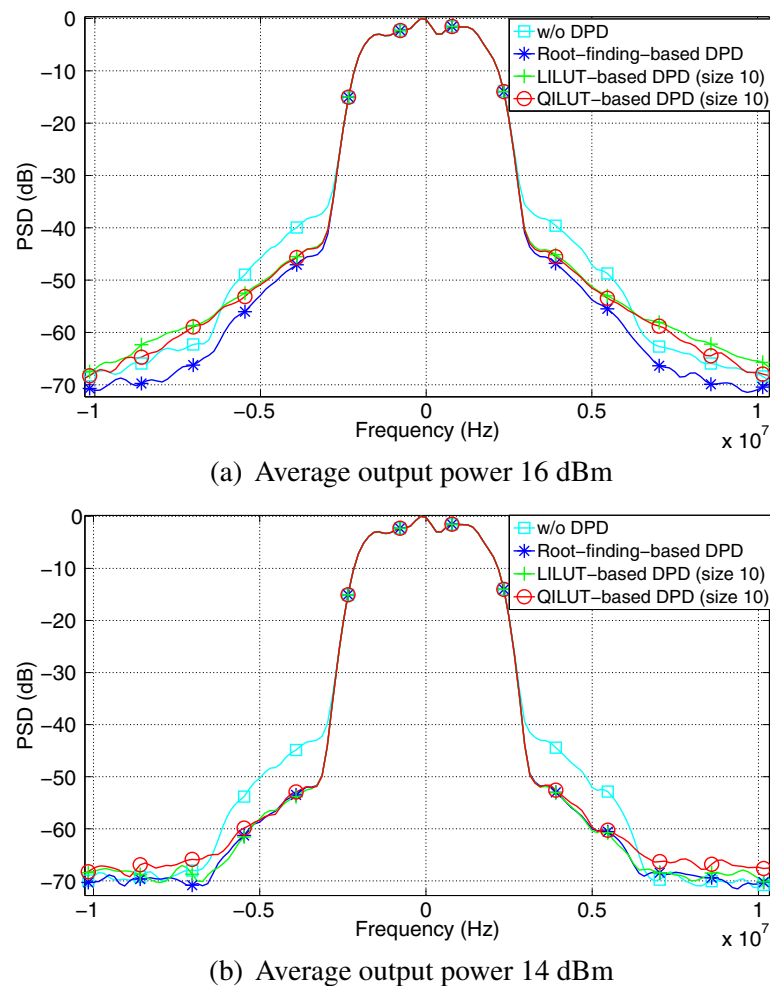


Fig. 16 Comparison of LILUT-based DPD and QILUT-based DPD

of the condition number and considering the influence of the number of bits of ADC and noise in the signal measurement, it shows that DLA is more robust than ILA with respect to perturbations. The LUT-based, LILUT-based, and QILUT-based DPDs are then proposed for PA linearization based on MP model with DLA. These three DPDs allow some tradeoff between the linearization performance, time efficiency and table size. In different applications, a more appropriate DPD can be chosen to fit the actual situation. Moreover, the hardware condition of experimental setup is discussed. If a more accurate results are expected, a higher bits of ADC and a wider bandwidth of instrument are required.

Competing interests

This work is original research that has not been published previously, and not under consideration for publication elsewhere, in whole or in part.

Acknowledgements

This work was supported by the China Scholarship Council, the grant from Science and Technology Planning Project of Guangdong Province, China (No.

2015A050502011), the grant from National Natural Science Foundation of China (No. 61401157) and the grant from the funds of central universities (No. 2015ZM127).

Author details

¹CNRS UMR6164, IETR, Ecole Polytechnique de l'universite de Nantes, Rue Christian Pauc, Nantes, France. ²The 54th Research Institute of China Electronics Technology Group Corporation, Shijiazhuang, Peoples Republic of China. ³Sino-French Research Center in Information and Communication (SFC/RIC), Rue Christian Pauc, Nantes, France. ⁴IUT, GEII Nantes, Site Fleuriaye, Av. du Prof J. Rouxel, Carquefou, France. ⁵School of Electronic and Information Engineering, South China University of Technology, Wushan Road, Tianhe District, Guangzhou, Peoples Republic of China. ⁶School of Computer Science and Engineering, South China University of Technology, Wushan Road, Tianhe District, Guangzhou, Peoples Republic of China.

Received: 9 December 2015 Accepted: 29 April 2016

Published online: 10 May 2016

References

1. FM Ghannouchi, O Hammi, Behavioral modeling and predistortion. *IEEE Microw. Mag.* **10**(7), 52–64 (2009)
2. M Hassan, LE Larson, VW Leung, DF Kimball, PM Asbeck, A wideband CMOS/GaAs HBT envelope tracking power amplifier for 4G LTE mobile

- terminal applications. *IEEE Trans. Microw. Theory Tech.* **60**(5), 1321–1330 (2012)
3. O Hammi, A Kwan, S Bensmida, KA Morris, FM Ghannouchi, A digital predistortion system with extended correction bandwidth with application to LTE-A nonlinear power amplifiers. *IEEE Trans. Circuits Syst. I Regular Papers.* **61**(12), 3487–3495 (2014)
 4. M Abi Hussein, VA Bohara, O Venard, in *International Symposium on Wireless Communication Systems (ISWCS)*. On the system level convergence of ILA and DLA for digital predistortion (IEEE, Paris, 2012), pp. 870–874. doi:10.1109/ISWCS.2012.6328492
 5. H Paaso, A Mammela, in *Proc. IEEE Int. Symp. on Wireless Communication Systems*. Comparison of direct learning and indirect learning predistortion architectures, (2008), pp. 309–313
 6. DR Morgan, Z Ma, L Ding, in *Proc. IEEE Int. Conference on Communications*. Reducing measurement noise effects in digital predistortion of RF power amplifiers, vol. 4 (IEEE, 2003), pp. 2436–2439. doi:10.1109/ICC.2003.1204371
 7. L Ding, GT Zhou, DR Morgan, Z Ma, JS Kenney, J Kim, CR Giardina, A robust digital baseband predistorter constructed using memory polynomials. *IEEE Trans. Commun.* **52**(1), 159–165 (2004)
 8. J Kim, K Konstantinou, Digital predistortion of wideband signals based on power amplifier model with memory. *Electron. Lett.* **37**(23), 1417–1418 (2001)
 9. D Zhou, VE DeBrunner, Novel adaptive nonlinear predistorters based on the direct learning algorithm. *IEEE Trans. Signal Process.* **55**(1), 120–133 (2007)
 10. E Cottais, Y Wang, S Toutain, A new adaptive baseband digital predistortion technique. *Eur. Microw. Assoc.* **2**, 154–159 (2006)
 11. N Naskas, Y Papananos, Neural-network-based adaptive baseband predistortion method for RF power amplifiers. *IEEE Trans. Circuits Syst. II Exp. Briefs.* **51**(11), 619–623 (2004)
 12. F Mkaem, S Boumaiza, Physically inspired neural network model for RF power amplifier behavioral modeling and digital predistortion. *IEEE Trans. Microw. Theory Tech.* **59**(4), 913–923 (2011)
 13. F Li, B Feuvrie, Y Wang, W Chen, MP/LUT baseband digital predistorter for wideband linearisation. *Electron. Lett.* **47**(19), 1096–1098 (2011)
 14. R Singla, S Sharma, Low complexity look up table based adaptive digital predistorter with low memory requirements. *EURASIP J. Wirel. Commun. Netw.* **2012**(1), 43 (2012)
 15. R Singla, S Sharma, Digital predistortion of power amplifiers using look-up table method with memory effects for LTE wireless systems. *EURASIP J. Wirel. Commun. Netw.* **2012**(1), 330 (2012)
 16. H Li, DH Kwon, D Chen, Y Chiu, A fast digital predistortion algorithm for radio-frequency power amplifier linearization with loop delay compensation. *IEEE J. Sel. Top. Signal Process.* **3**(3), 374–383 (2009)
 17. B Fehri, S Boumaiza, Baseband equivalent Volterra series for behavioral modeling and digital predistortion of power amplifiers driven with wideband carrier aggregated signals. *IEEE Trans. Microw. Theory Tech.* **62**(11), 2594–2603 (2014)
 18. C Eun, EJ Powers, A new Volterra predistorter based on the indirect learning architecture. *IEEE Trans. Signal Process.* **45**(1), 223–227 (1997)
 19. DR Morgan, ZX Ma, J Kim, MG Zierdt, J Pastalan, A generalized memory polynomial model for digital predistortion of RF power amplifiers. *IEEE Trans. Signal Process.* **54**(10), 3852–3860 (2006)
 20. A Zhu, JC Pedro, TR Cunha, Pruning the Volterra series for behavioral modeling of power amplifiers using physical knowledge. *IEEE Trans. Microw. Theory Tech.* **55**(5), 813–821 (2007)
 21. X Feng, B Feuvrie, AS Descamps, Y Wang, Improved baseband digital predistortion for linearizing PAs with nonlinear memory effects using linearly interpolated LUT. *Electron. Lett.* **49**(22), 1389–1391 (2013)
 22. X Feng, B Feuvrie, AS Descamps, Y Wang, A digital predistortion technique based on non-uniform MP model and interpolated LUT for linearizing PAs with memory effects. *Electron. Lett.* **50**(24) (2014)
 23. X Feng, B Feuvrie, AS Descamps, Y Wang, in *IEEE Topical Conference on Power Amplifiers for Wireless and Radio Applications (PAWR)*. A digital predistortion method based on nonuniform memory polynomial model using interpolated LUT (IEEE, San Diego, CA, 2015), pp. 1–3. doi:10.1109/PAWR.2015.7139201
 24. E Cottais, Y Wang, in *The Third International Conference on Digital Telecommunications, ICDT'08*. Influence of instruments bandwidth in the power amplifier linearization process (IEEE, Bucharest, 2008), pp. 11–14
 25. J Kwon, C Eun, in *International Journal of Intelligent Systems Technologies and Applications archive*. Digital feedforward compensation scheme for the nonlinear power amplifier with memory, vol. 9 (Inderscience Publishers, Geneva, Switzerland, 2010), pp. 326–334. doi:10.1504/IJISTA.2010.036586
 26. F Li. Linéarisation des amplificateurs de puissance dans les systèmes de communication large bande par prédistorsion numérique en bande de base. PhD thesis (Université de Nantes, Nantes, French, 2012). https://www.ietr.fr/IMG/pdf/Couv_RV_LL_Feng.pdf

Submit your manuscript to a SpringerOpen[®] journal and benefit from:

- Convenient online submission
- Rigorous peer review
- Immediate publication on acceptance
- Open access: articles freely available online
- High visibility within the field
- Retaining the copyright to your article

Submit your next manuscript at ► springeropen.com